JTE HCMUTE
ISSN: 2615-9740

JOURNAL OF TECHNICAL EDUCATION SCIENCE
Ho Chi Minh City University of Technology and Education
Website: https://jte.edu.vn
Email: jte@hcmute.edu.vn

An Improved Control Method for Direct Torque Control Based on Sliding Mode Control

Thi-Hong-Huong Ngo[1*], Minh-Tam Nguyen[2], Vinh-Quan Nguyen[2]
[1]*Dong An Polytechnic, Vietnam*
[2]*Ho Chi Minh City University of Technology and Education, Vietnam*

[*]Corresponding author. *Email: ngothihonghuong1992@gmail.com*

ARTICLE INFO

Received: 31/10/2023
Revised: 17/11/2023
Accepted: 08/12/2023
Published: 28/04/2024

KEYWORDS

Direct Torque Control;
Sliding Mode Control;
Induction motor;
Nonlinear Systems;
Third-order cascade inverter.

ABSTRACT

This paper presents an improved method of direct torque control (DTC) for three–phase asynchronous motors with squirrel cage rotors. The improved method of DTC uses three sliding mode controllers to control torque and flux independently. From simulation and experimentation in real time RT, using Sim Power Systems of matlab-simulink through RT-LAB compiler, hardware simulation algorithm in HIL- Hardware-in-the-Loop by OPAL-RT device for the three-phase asynchronous induction motor, this is the new algorithm presented in the article. The three-phase asynchronous induction motor 1-hp, 150 rad/s with a three-phase three-level cascade inverter, the results show the estimated speed and the good tracking speed according to the value set at a frequency varying from the lowest 3 rad/s to the highest 150 rad/s, and the system remains stable when the stator and rotor resistance changes up to 1.5 times the initial value in the presence of noise. Simulation during execution, so simulation results and experimental results are very consistent. On the other hand, using a multi-level inverter with the new PM modulation algorithm increases the system's sustainability compared to the two-level inverter used in previously published articles. The results also show that using a sliding surface with a nonlinear function that has been proven to be Lyapunov stable significantly reduces the moment chattering phenomenon compared to previous algorithms using DTC control.

Doi: https://doi.org/10.54644/jte.2024.1491

1. Introduction

For many years, the field of electric drive control of squirrel cage three-phase AC electric motor has been researched by scientists, from classic theories to modern techniques [1]. Currently, asynchronous motor control has achieved great developments. The improvements and perfections of the inverters have partly met the strict requirements in automatic adjustment, and new features have been added to the inverter to suit the high performamance control needs in practice.

The control of asynchronous motor speed has attracted the interest of many researchers. Control methods have been proposed and verified by simulation such as the magnetic directional control method FOC, classical DTC and improved DTC in which DTC uses carrier pulse width modulation [2] shows many outstanding advantages and are commonly applied.

Although the DTC control method was discovered several decades ago, due to some limitations in terms of equipment, it was not until recent years that practical applications were developed. The DTC method is based on the direct effect of the voltage vector on the stator ring hook magnetic flux, changing the stator magnetic flux vector state results in a direct change to the electromagnetic moment of the motor. This is a simple control method, less dependent on motor parameters, fast and flexible moment response [3].

Currently in the country, there are many studies using the DTC control method for three-phase asynchronous motors based on sliding control applied in electric vehicles, but they all use two inverters and intermittent sliding surfaces, so the current and moment are strongly motivated. The article uses a third-level inverter and instead interrupts it with a nonlinear (tanh(s) function), so it improves the

compatibility in current and moment. To achieve the best results compared to the requirements, this article will combine with the direct moment control method squirrel cage rotor three-phase asynchronous motor based on sliding control base (SMC) with third-order cascade inverter, using hardware simulation algorithm in HIL- Hardware-in-the-Loop by OPAL-RT device for the three-phase asynchronous induction motor. On the other hand, using a multi-level inverter with the new PM modulation algorithm increases the system's sustainability compared to the two-level inverter. Research by Emelyanov, Utkins, and Itkis in the 1950s suggested a variable structure control model and sliding mode control for nonlinear systems, but due to the use of a delay comparator, it will generate very large harmonics in torque and current, which depends a lot on how the inverter is controlled [4], [5].

Sliding mode control is an effective simple control method, based on feedback of state variables of the system [5], as well as a third-order cascade inverter has a phase modulated carrier (PM- Phase Modulation) to reduce total harmonic distortion (THD) in torque and current and to reduce the common mode voltages CMV, in order to achieve the best possible result. The key to SMC is to reduce the complexity of higher order systems, through the selection of the sliding function and its derivative (also known as the sliding surface) [6]. The outstanding advantages of SMC are fast response time, no overshoot, no oscillation, zero speed setting error, in addition, the controller has high nominal quality [7] - [16].

But in this method, there is also a small disadvantage that the phenomenon of oscillation around the sliding surface (chattering phenomenon), the chattering phenomenon arising in the sliding control is also proposed by many scientists to overcome the problem. This paper will use nonlinear sliding surface to reduce chattering phenomenon.

2. Main contents

Table 1. *Symbols*

Symbol	Unit	Note
R_s, R_r	Ω	Stator, rotor resistance
L_s, L_r	H	Stator, rotor inductance
L_m	H	Mutual inductance
u_{sq}, u_{sd}	V	Stator voltages (d-q axis)
u_{rq}, u_{rd}	V	Rotor voltages (d-q axis)
i_{sq}, i_{sd}	A	Stator currents (d-q axis)
i_{rq}, i_{rd}	A	Rotor currents (d-q axis)
φ_{sq}, φ_{sd}	Wb	Stator fluxes (d-q axis)
φ_{rq}, φ_{rd}	Wb	Rotor fluxes (d-q axis)
ω_r	rad/s	Angular velocity
T_e, T_m	N.m	Electromagnetic, load torque
p	Pole pairs	Pole-pairs
J	Kg.m2	Inertia constant
B	N.m.s	Friction coefficient
IGBT		Transistor with isolated control pole
PWM		Pulse width modulation
DSP		Digital signal processing
DTC		Direct torque control
FOC		Flux directional control
SMC		Sliding mode control

JTE
HCMUTE
ISSN: 2615-9740

JOURNAL OF TECHNICAL EDUCATION SCIENCE
Ho Chi Minh City University of Technology and Education
Website: https://jte.edu.vn
Email: jte@hcmute.edu.vn

2.1. Engine model in d-q coordinate system

Figure 1 shows a three-phase asynchronous motor in d-q coordinates [11], [12]

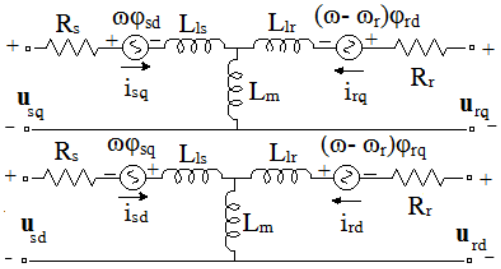

Figure 1. *Model of a motor in the d-q coordinate.*

The stator and rotor potential nonlinear equations of squirrel cage rotor asynchronous motors in the d-q coordinate system are presented as the following matrix:

$$\begin{bmatrix} u_{sd} \\ u_{sq} \end{bmatrix} = \begin{bmatrix} R_s & 0 \\ 0 & R_s \end{bmatrix} \begin{bmatrix} i_{sd} \\ i_{sq} \end{bmatrix} + \frac{d}{dt} \begin{bmatrix} \varphi_{sd} \\ \varphi_{sq} \end{bmatrix} + \begin{bmatrix} 0 & -\omega_e \\ \omega_e & 0 \end{bmatrix} \begin{bmatrix} \varphi_{sd} \\ \varphi_{sq} \end{bmatrix} \tag{1}$$

$$\begin{bmatrix} 0 \\ 0 \end{bmatrix} = \begin{bmatrix} R_r & 0 \\ 0 & R_r \end{bmatrix} \begin{bmatrix} i_{rd} \\ i_{rq} \end{bmatrix} + \frac{d}{dt} \begin{bmatrix} \varphi_{rd} \\ \varphi_{rq} \end{bmatrix} + \begin{bmatrix} 0 & -(\omega_e - p\omega_r) \\ (\omega_e - p\omega_r) & 0 \end{bmatrix} \begin{bmatrix} \varphi_{sd} \\ \varphi_{sq} \end{bmatrix} \tag{2}$$

with

$$\begin{bmatrix} \varphi_{sd} \\ \varphi_{sq} \end{bmatrix} = \begin{bmatrix} L_s & 0 \\ 0 & L_s \end{bmatrix} \begin{bmatrix} i_{sd} \\ i_{sq} \end{bmatrix} + \begin{bmatrix} L_m & 0 \\ 0 & L_m \end{bmatrix} \begin{bmatrix} i_{rd} \\ i_{rq} \end{bmatrix} \tag{3}$$

$$\begin{bmatrix} \varphi_{rd} \\ \varphi_{rq} \end{bmatrix} = \begin{bmatrix} L_m & 0 \\ 0 & L_m \end{bmatrix} \begin{bmatrix} i_{sd} \\ i_{sq} \end{bmatrix} + \begin{bmatrix} L_r & 0 \\ 0 & L_r \end{bmatrix} \begin{bmatrix} i_{rd} \\ i_{rq} \end{bmatrix} \tag{4}$$

$$T_e = \frac{3}{2} p \begin{bmatrix} \varphi_{sd} & \varphi_{sq} \end{bmatrix} \begin{bmatrix} i_{sq} \\ -i_{sq} \end{bmatrix} \tag{5}$$

$$J \frac{d\omega_r}{dt} = \left(T_e - T_m - B\omega_r \right) \tag{6}$$

$$\omega_r = \frac{d\theta}{dt} \tag{7}$$

The symbols of the motor are given in table 1, if a reference frame attached to the stator magnetic flux vector is selected, the angular speed of rotation of the coordinate axis system is equal to the angular speed of rotation of the stator magnetic flux vector, and the D-axis of the coordinate axis coincides with the stator magnetic flux vector, we have:

$$\varphi_{sq} = \dot{\varphi}_{sq} = 0 \tag{8}$$

$$u_{sq} = R_s i_{sq} + \omega_r \varphi_{sd} \tag{9}$$

$$u_{sd} = R_s i_{sd} + \dot{\varphi}_{sd} \tag{10}$$

$$T_e = \frac{3}{2} p \left(\varphi_{sd} i_{sq} \right) \tag{11}$$

$$\varphi_{sd} = \int \left(u_{sd} - R_s i_{sd} \right) dt \tag{12}$$

2.2. Sliding control system design

2.2.1. Sliding controller design for magnetic flux

The equation (10), we have:

$$\dot{\varphi}_{sd} = u_{sd} - R_s i_{sd} \tag{13}$$

The equation (9), we have:

$$\omega_r \varphi_{sd} = u_{sq} - R_s i_{sq} \tag{14}$$

From the general equation define the slip surface as:

$$s(x) = \left(\frac{d}{dt} + c\right)^{n-1} e \tag{15}$$

Here constant c > 0, e is the error and n are the number of orders in the system.

Since the system has n = 1, choose the slide as equation (14) with c_F>0 to satisfy the Hurwitz stability condition:

$$s_F(t) = c_F e_F \tag{16}$$

With $e_F = \varphi_{sd}^* - \varphi_{sd}$, in which φ_{sd} is the stator flux estimated from equation (12), and φ_{sd}^* is the set flux.

Sliding face derivatives, we get:

$$\dot{s}_F(t) = c_F \dot{e}_F = c_F\left(\dot{\varphi}_{sd}^* - \dot{\varphi}_{sd}\right) \tag{17}$$

Substitution of equation (13) into (17):

$$\dot{s}_F = -c_F\left(u_{sd} - R_s i_{sd}\right) + c_F \dot{\varphi}_{sd}^* \tag{18}$$

The proposed rules of control for magnetic flux are:

$$u_{sd} = \frac{1}{c_F}\left(\varepsilon_F \tanh\left(s_F/\delta\right)\right) + \dot{\varphi}_{sd}^* + R_s i_{sd} \tag{19}$$

2.2.2. Sliding controller design for the torque

Sliding mode control laws for velocity

The equation (6), we infer:

$$\dot{\omega}_r = \frac{1}{J}\left(T_e - T_m - B\omega_r\right) \tag{20}$$

Similarly, because of the first – order system, the slip surface for the moment should be chosen as:

$$s_M(t) = c_M e_M \tag{21}$$

However, to increase the setup time for the system, the sliding function can be chosen as follows:

$$s_M(t) = c_M e_M(t) + k_{iM}\int e_M(t)dt \tag{22}$$

With c_M, k_{iM} > 0 to satisfy the Hurwitz stability condition, error $e_M = \omega_r^* - \omega_r$ which in that ω_r^* is the set speed and ω_r is the speed of the motor.

Sliding surface derivative:

$$\dot{s}_M(t) = c_M(\dot{\omega}_r^* - \dot{\omega}_r) + k_{iM} e_M \tag{23}$$

Substitute equation (20) into (23)

$$\dot{s}_M(t) = c_M \dot{\omega}_r^* - \frac{c_M}{J}\left(T_e - T_m - B\omega_r\right) + k_{iM} e_M(t) \tag{24}$$

Proposed control law for moment:

$$T_e = \frac{J}{c_M}\left(\varepsilon_M \tanh\left(s_M/\delta\right) + k_{iM} e_M\right) + J\dot{\omega}_r^* + T_m + B\omega_r \tag{25}$$

Sliding control law for u_{sq}

Similarly, because the system is first – order and to increase the setup time for the system, the sliding function is chosen as follows:

$$s_T(t) = c_T e_T(t) + k_{iT}\int e_T(t)dt \tag{26}$$

With $e_T = T_m^* - T_e$ in which T_m^* is the setting moment and T_e is the motor torque estimated from the equation (11)

Sliding surface derivative:

$$\dot{s}_T(t) = c_T \dot{e}_T + k_{iT}\left(T_m^* - T_e\right) \tag{27}$$

Substituting equation (9, 11) into (28), we have:

$$\dot{s}_T(t) = c_T \dot{e}_T + k_{iT} T_m^* - k_{iT}\frac{3}{2} p \frac{i_{sq}}{\omega_r}\left(u_{sq} - R_s i_{sq}\right) \tag{28}$$

The control law is recommended as:

$$u_{sq} = \frac{2}{3pk_{iT}}\frac{\omega_r}{i_{sq}}\left(c_T \dot{e}_T + k_{iT} T_m^* + \varepsilon_T \tanh(s_T/\delta)\right) + R_s i_{sq} \tag{29}$$

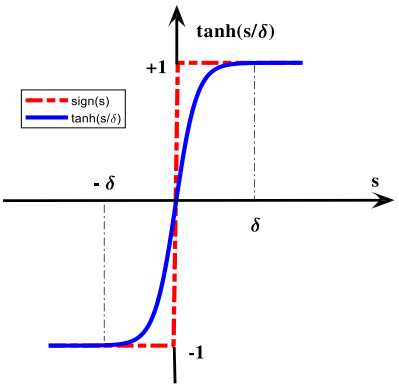

Figure 2. *Sign function and tanh function.*

Figure 2 shows the response of the sign function intermittently (distinct red) and continuous tanh function (blue), δ>0 to satisfy the Hurwitz stability condition.

The authors suggest to use tanh continuous function instead of sign discontinuity function to reduce oscillations around the sliding surface.

2.3. Third-order cascade inverter and PM modulation

Figure 3 illustrates third-order cascade inverter structure and H-bridge diagram for one phase consisting of four IGBT-Insulated Gate Bipolar Transistor locks, we have:

JTE
HCMUTE
ISSN: 2615-9740

JOURNAL OF TECHNICAL EDUCATION SCIENCE
Ho Chi Minh City University of Technology and Education
Website: https://jte.edu.vn
Email: jte@hcmute.edu.vn

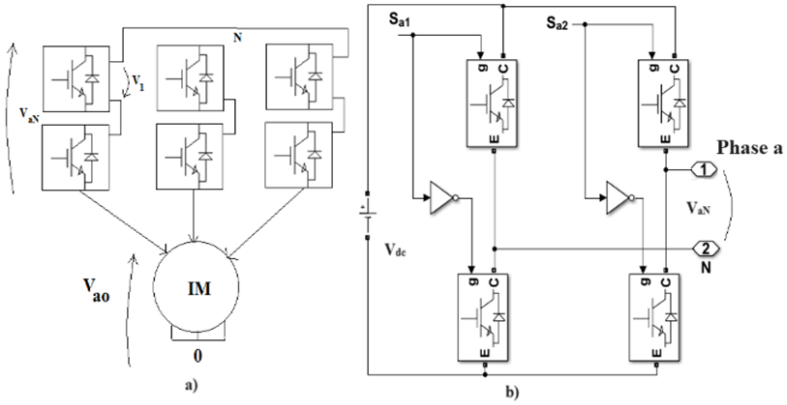

Figure 3. *a) Third-order cascade inverter structure. b) H-bridge for a phase.*

$$V_{a0} = V_{aN} + V_{N0} \quad (30)$$

where V_{cm} is common – mode voltage (CMV)

$$V_{N0} = V_{cm} = (V_{aN} + V_{bN} + V_{cN}) \quad (31)$$

Let n = 3, be the number of steps of the inverter, and the V_{dc} sources are the same, we have a table of switching status of corresponding locks for continuous output voltage from [-1V_{dc}, 0, +1V_{dc}] as shown in Table 2 .

Table 2. *Switching status of a phase*

n	**S_{a1}, S_{a2}**	**Output Voltage = (S_{a1} - S_{a2})*V_{dc}**
0	[0, 1]	-1V_{dc}
1	[0, 0], [1, 1]	0
2	[1, 0]	+1V_{dc}

Figure 4 shows the PM carrier modulation model for the inverter, with the control signals g(t) and G(t) given by equation (32).

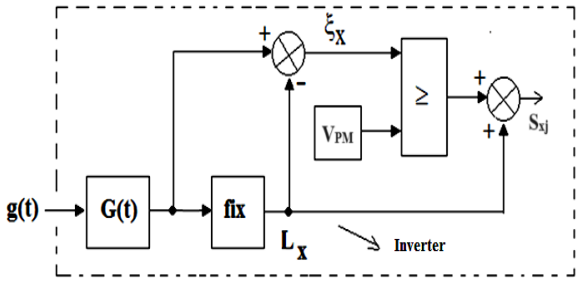

Figure 4. *The PM carrier modulation.*

$$G(t) = \left(g(t) + 1\right)\frac{n - 1}{2} \quad (32)$$

The two components of the voltage G(t) are ξ_x, L_x, in which, $\leq L_x \leq n - 2$ is the integer part of the signal G(t), given by equation (33), $0 \leq \xi_x \leq 1$ is the remainder after division, given by equation (34), n = 3, is the number of steps of the inverter, S_{xj} the state of the key is given in Table 2 and V_{PM} is the carrier wave after PM modulation.

$$L_X = \begin{cases} n\text{-}2, \text{ khi } G(t) \geq n\text{-}2 \\ fix(G(t)), \text{ otherwise} \end{cases} \quad (33)$$

$$\xi_x = G(t) - L_x \quad (34)$$

Consider high-frequency waves as equation (35):

$$e(t) = A_c\cos(\omega_c t + \varphi),\ \omega_c = 2\pi f_c \quad (35)$$

The carrier wave without modulation as equation (36), with $A_c = 1$

$$c(t) = \frac{2}{\pi}\sin^{-1}\left(e(t)\right) = \frac{2}{\pi}\sin^{-1}\left(A_c\cos\left(\omega_c t + \varphi\right)\right) \quad (36)$$

The carrier wave has been normalized by equation (37):

$$V_C(t) = \frac{\max(c(t)) + c(t)}{\max(c(t)) - \min(c(t))} \quad (37)$$

where max and min are the largest and smallest amplitudes of c(t).

Call the control signal as equation (38):

$$g(t) = E_m\sin(\omega_m t),\ \omega_m = 2\pi f_m \quad (38)$$

From the high frequency wave e(t), if the phase angle φ changes according to the control signal g(t), we have PM phase modulation.

$$e_{PM}(t) = A_c\cos[\omega_c t + (m_{px}/E_m)g(t)] \quad (39)$$

where $\theta = \omega_c t + (m_{px}/E_m)g(t)$, m_{px} modulation index, with x = a, b, c.

Substituting into equation (36-37), we have PM phase-modulated carrier.

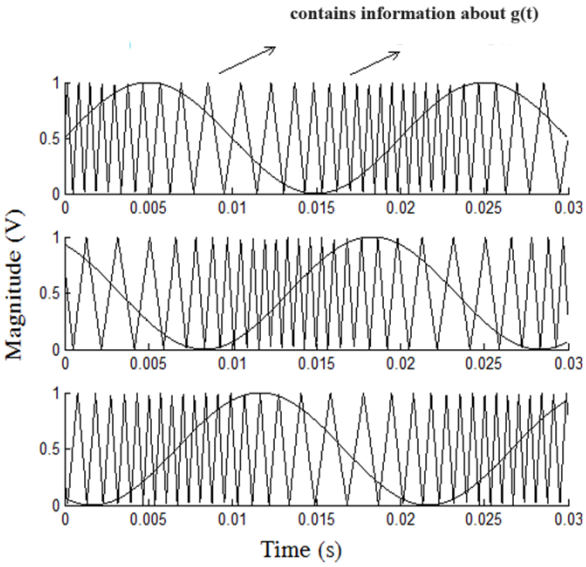

Figure 5. *Carrier wave with PM modulation.*

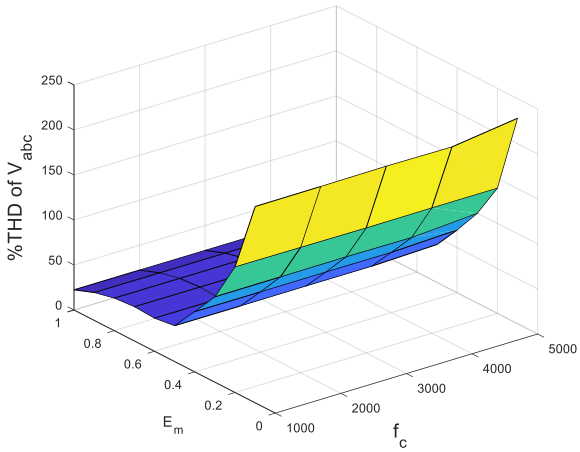

Figure 6. *The impact of E_m and carrier frequency f_c on the average %THD.*

Figure 5, shows the PM modulation carrier with frequency f_c = 1KHz, modulation index $m_{px} = 5$, the PM modulation carrier has a frequency that contains completely the information of the control signal g(t). So that IGBT switch is easy to completely recover the control signal from the carrier.

Figure 6 shows the impact of E_m and carrier frequency f_c on the average %THD of current i_x (x = a, b, c). When the inverter has a motor load, the %THD of i_x increases rapidly, increasing E_m from 0 to 1, while increasing the carrier frequency f_c from 1KHz to 5KHz reduces the %THD of i_x. Therefore, the E_m index and the carrier frequency f_c will affect the performance of the PM modulation algorithm over the entire operating range of the inverter.

3. Results and Discussion

With Matlab/Simulink as the simulation software and a sampling time of T_s = 40 μs the simulation and experimental results are evaluated in combination with a third-order cascade inverter with PM modulated carrier wave for the motor described in Table 3.

Table 3. *Parameters of the motor*

Wattage	1HP, 50 Hz
Wire voltage	380 (V)
Speed	150 (ras/s)
Moment T_m	5 (N.m)
R_s, L_s	1.177 (Ω), 10(mH)
R_r, L_r	1.383 (Ω) ,10(mH)
p	2
J	0.005 (kg.m^2)

3.1. Simulation results

Figure 7 shows a schematic diagram of direct torque control, consisting of a controller for flux, and two controllers for speed.

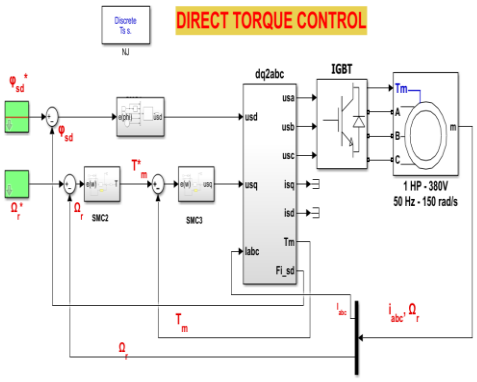

Figure 7. *Simulation diagram.*

Figure 8a, Wire voltage V_{ab}, Voltage CMV; Figure 8b, phase voltage V_{an}; Figure 8c is FFT of V_{ab} of the third-order cascade inverter, with THD = 35.28%.

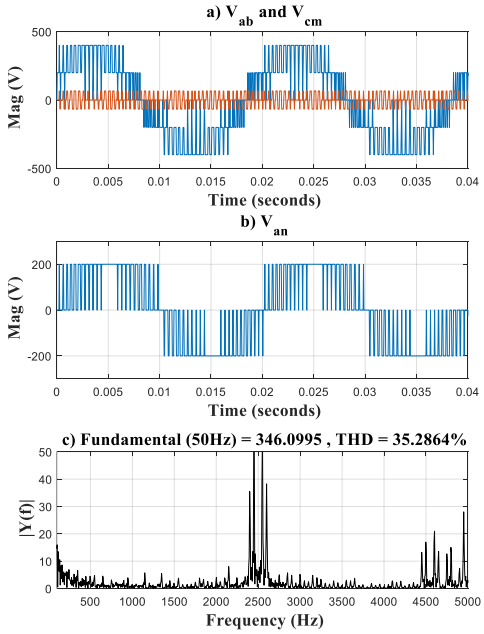

Figure 8. *a) Line voltage V_{ab} and Voltage V_{cm}; b) Phase voltage V_{an}; c) FFT of V_{ab}.*

JTE HCMUTE
ISSN: 2615-9740
JOURNAL OF TECHNICAL EDUCATION SCIENCE
Ho Chi Minh City University of Technology and Education
Website: https://jte.edu.vn
Email: jte@hcmute.edu.vn

Figures 9 and Figures 10 are the four waveforms of the motor when R_s=1.177 Ω, R_r =1.383 Ω

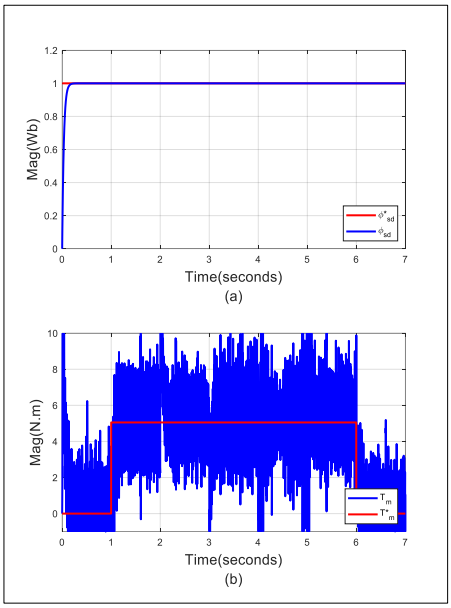

Figure 9. *a) Measured flux φ_{sd} and set flux φ^*_{sd}; b) Measured moment T_m and set moment T^*_m*

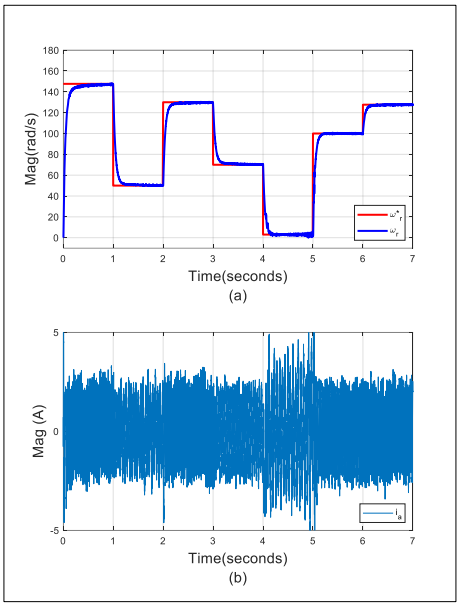

Figure 10. *a) Measuring speed ω_r and set speed ω^*; b) Current i_{sa}.*

Figure 9a shows the measured flux φ_{sd} (blue line) closely following the applied flux φ^*_{sd} (red line), figure 9b shows the measured moment T_m (blue line) follow the setting moment T^*_m (red line), but at some point the speed changes suddenly the moment is overshoot.

Figure 10a shows that when the speed changes from a low 3 rad/s to a maximum of 150 rad/s, the measured value ω_r (blue line) follows the set value ω^*_r (red line), figure 10b shows that the phase a current reaches a value of about 2A at seconds (0-4) and (5-7), at the lowest value of 3 rad/s, the phase a current fluctuates light about 3A - 4A at sec (4-5).

Figure 11 and figure 12 are four waveforms of the motor, when increasing the R_s value by 2 times and the value of R_r by 1.5 times, we have R_s= 2,354 Ω, R_r = 2.073 Ω.

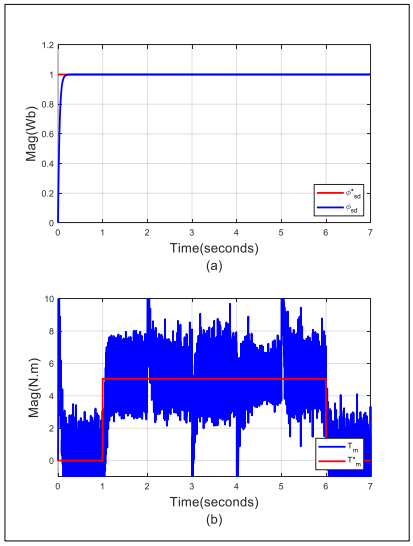

Figure 11. *a) Measured flux φ_{sd} and set flux φ^*_{sd}; b) Measured moment T_m and set moment T^*_m*

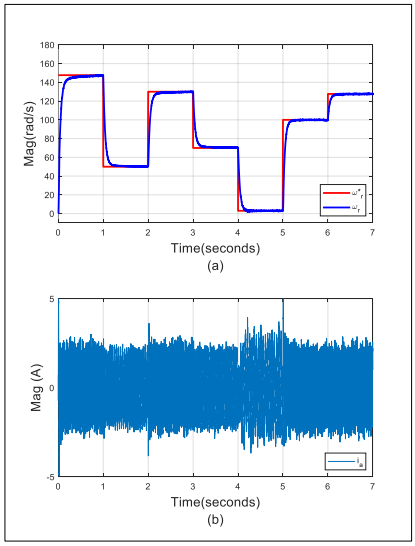

Figure 12. *a) Measuring speed ω_r and set speed ω^*_r; b) Current i_{sa}*

When increasing the R_s value and the value of R_r by 1.5 times, Figure 11a shows that the measured flux still follows the set flux, Figure 11b shows that the measured moment follows the set moment, at some point the speed changes suddenly, the moment is still slightly overstated.

When increasing the value of R_s and the value of R_r by 1.5 times, Figure 12a shows that when the velocity changes from low to high, the measured value ω_r still follows the value ω^*_r, at the lowest value of 3 rad/s, the phase a current fluctuates slightly.

Figure 12b shows that the phase a current reaches a value of about 2A at seconds (0-4) and (5-7), phase a current reaches a value of about 2.5A at sec (4-5).

Figure 13 is the stator flux vector φ_s when controlling the improved DTC on the basis of the slip control for a three – phase asynchronous motor with parameters given in Table 1.

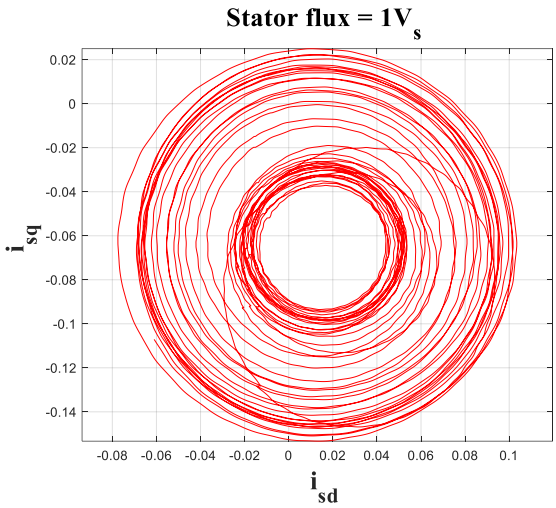

Figure 13. *Simulation for the stator flux vector φ_s*

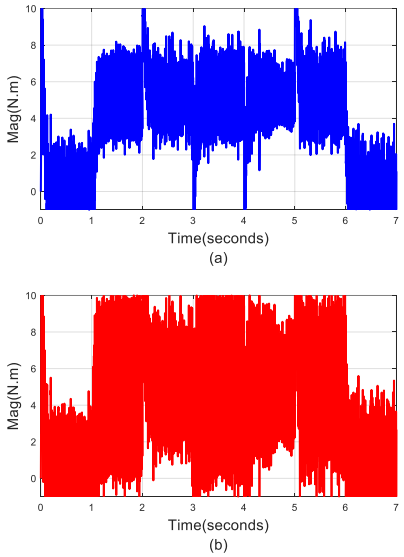

Figure 14. *a) Moment estimated with tanh(s); b) Moment estimated with function sgn(s).*

Figure 14 is the moment estimated from Equation (11), which shows that when the sliding surface uses the continuous function tanh(s) there is a significant reduction in chattering compared to when using the discontinuity function sgn(s).

This leads to a decrease in the switching frequency of the IBGT keys, a decrease in the common mode voltage and a decrease in the output harmonics, which increases the stability of the controller.

Chattering can also cause damage to control objects or mechanical transmission systems, for example.

3.2. Experimental results

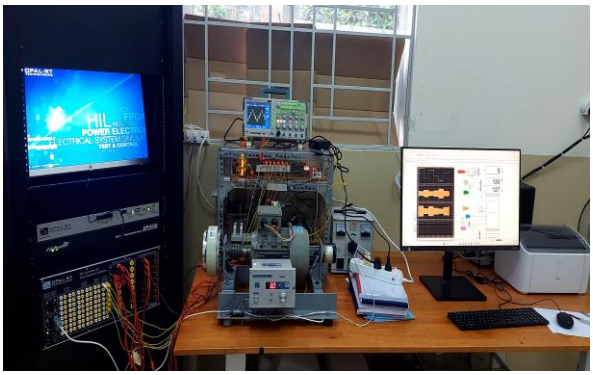

Figure 15. *A model of the experimental model with OPAL-RT*

JTE
HCMUTE
ISSN: 2615-9740

JOURNAL OF TECHNICAL EDUCATION SCIENCE
Ho Chi Minh City University of Technology and Education
Website: https://jte.edu.vn
Email: jte@hcmute.edu.vn

In this experiment, the OPAL-RT device is used to experiment on three phase asynchronous motors with squirrel cage rotors with parameters given in Table 3. The experimental period is 350 seconds divided equally into seven intervals, with results collected via the persional computer, as depicted in Figure 15.

It is the 1024 pulse encoder which provides the motor speed, and the LEM LF305-S sensor which provides the current i_x (x = a, b, c).

Figure 16, shows the experiment for line voltage V_{ab}, voltage V_{cm} , phase voltage V_{an} and spectrum of line voltage corresponding to applied moment T^*_m = 5 N.m with THD = 39.75%.

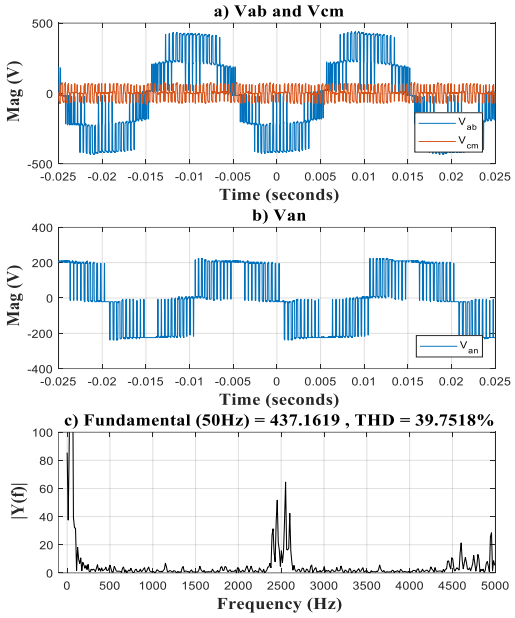

Figure 16. *Experiment with* T^*_m = 5 N.m, *a)* V_{ab}, V_{cm}, *b)* V_{an} *and c) FFT of* V_{ab}

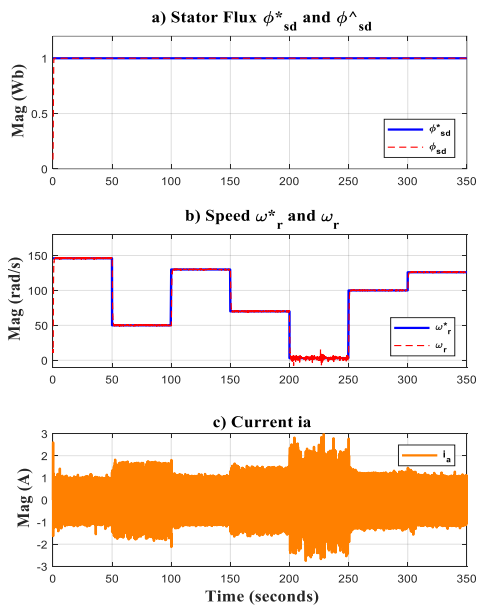

Figure 17. *Experimental results correspond to* $T_e^* = 5N.m$*: a) Flux* φ_{sd}^* *and estimated flux* $\hat{\varphi}_{sd}$*, b) speed* ω_r^* *and measured speed* ω_r*, c) Phase current* i_a

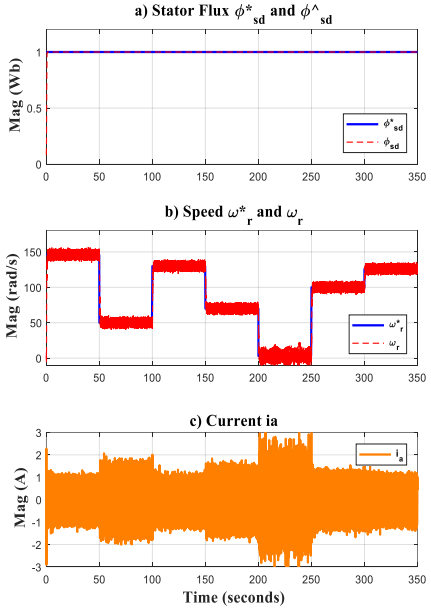

Figure 18. *Experimental results correspond to* $T_e^* = 5N.m$ *with the participation of noise: a) Flux* φ_{sd}^* *and estimated flux* $\hat{\varphi}_{sd}$ *,b) speed* ω_r^* *and measured speed* ω_r*, c) Phase current* i_a

JTE
HCMUTE
ISSN: 2615-9740

JOURNAL OF TECHNICAL EDUCATION SCIENCE
Ho Chi Minh City University of Technology and Education
Website: https://jte.edu.vn
Email: jte@hcmute.edu.vn

Figure 17a, experimental results corresponding to T^*_m = 5 N.m, shows that the set flux φ^*_{sd} and the estimated flux $\hat{\varphi}_{sd}$ coincide.

Using the data from Figure 17b, it can be seen that the measured velocity ω_r follows the set speed ω^*_r well from the highest value to the lowest value. At the value of 3 rad/s, the measured velocity fluctuates strongly around the set value.

Figure 17c illustrates that the phase a stator current reaches a value of approximately 3A at the lowest velocity value (3 rad/s).

Figure 18, experimental results corresponding to $T^*_e = 5N.m$ with the presence of noise, show that the applied flux φ^*_{sd} and the estimated flux $\hat{\varphi}_{sd}$ coincide. The measured velocity ω_r still follows well with the applied velocity ω^*_r from the highest value of 150 rad/s to the lowest value of 3 rad/s (Figure 20b). Figure 18c, shows that the phase a stator current reaches a value of about 3A. At the lowest velocity value (3 rad/s), the current is still overshoot.

When the set speed $\omega^*_r = 150\ rad/s$, figure 25, shows the experiment for the stator flux vector φ_s

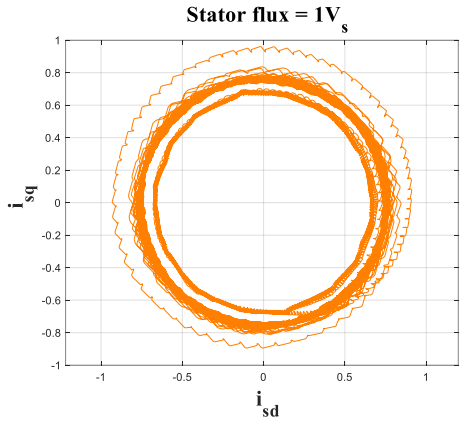

Figure 19. *Experiment when ω*$_r$ = 150 rad/s for word vector through stator φ_s*

4. Conclusions

This paper presents a method of direct torque control (DTC) for three – phase asynchronous motors based on slip control (SMC). Simulation results have shown that the tracking speed is good according to the set speed even when the speed varies from the highest value of 150 rad/s to the lowest value of 3 rad/s. The controller is still stable when increasing the resistor values R_s and R_r to 1.5 times the original value, the measuring speed still set speed from low to high. At the same time, the algorithm designed to control the DCT using HIL technology has improved the quality of current and torque. Flux and torque ripples are minimized to limit problems such as mechanical vibration, acoustic noise, temperature,…. Besides, the steady state error for the SSE-Steady State Error system has been improved. The new PM phase modulation algorithm has reduced the common-mode voltage, resulting in reduced electrical discharge around the motor shaft caused by this voltage, and reduced the number of times IGBT switches are turned on and off, improving the output quality of the inverter.

Acknowledgments

This work is supported by Ho Chi Minh City University of Technology and Education. The authors would like to express their sincere thanks to the editors and reviews for their many comments and appreciation.

Conflict of Interest

The authors declare no conflict of interest.

REFERENCES

[1] G. Majumdar and D. Medaule, "A new generation of intelligent power devices for motor drive applications," in *Fifth International Conference on Power Electronics and Variable-Speed Drives*, London, UK, 1994, pp. 35-41, doi: 10.1049/cp:19940936.

[2] K. B. Lee, Student Member,IEEE, Joong-Ho Song, Ick Choy, and Ji-Yoon Yoo,Member,IEEE, "Torque Ripple Reduction in DTC of Induction Motor Driven by Three-Level Inverter With Low Switching Frequency," *IEEE Transactions on Power Electronics*, vol. 17, no. 2, pp. 255-264, March 2002, doi: 10.1109/63.988836.
[3] V. N. Tien and N. D. Quan, "The direct control method of three-phase asynchronous motor torque," *Journal of science and technology*, Danang University, vol. 35, no. 6, 2009.
[4] P. Marino, M. D. Incecco, and N. Visciano, "Comparison of direct torque control methods for induction motors," *IEEE trans.*, 2001.
[5] G. Buja *et al.*, "Direct torque control of the application motor drive," *IEEE ISIE Conf. Rec*., 1997.
[6] J. Donlon *et al.*, "Sliding Mode Control with Observer and Application," *Professor, Dept. of EEE, St. Peter's University, Avadi, Chennai, Indi*, vol. 5, no. 10, 2016.
[7] N. T. H. Huong, "Three-phase asynchronous motor control by sliding mode control," Master's thesis, Ho Chi Minh City University of Technical Education, October, 2019.
[8] Q. Wu and C. Shao, "Novel Hybrid Sliding-mode Controller for Direct Torque Control Induction Motor Drives," *Proceedings of the American Control Conference Minneapolis*, Minnesota, USA, 2006, p. 2754-2758.
[9] V. Utkin, "Sliding mode and their application in variable structure systems", Moscow, 1978.
[10] V. Q. Nguyen, Q. T. Tran, and H. N. Duong, "Stator-flux-oriented control for three-phase induction motors using sliding mode control," *Journal of Electrical Systems*, p. 171-184, 2020.
[11] N. V. Quan and M. T. Long, "Sensorless sliding mode control method for a three-phase induction motor," *Electrical Engineering*, vol. 104, p. 3685–3695, 2022, doi: 10.1007/s00202-022-01578-5.
[12] Q. N. Vinh and T. P. T. Bich, "Sliding mode control of induction motor with fuzzy logic observer," *Electrical Engineering*, vol. 105, p. 2769–2780, 2023, doi: 10.1007/s00202-023-01842-2.
[13] N. V. Quan and M. T. Long, "Sliding mode control method for three-phase induction motor with magnetic saturation," *International Journal of Dynamics and Control*, vol. 12, pp.1522–1532, 2024, doi: 10.1007/s40435-023-01269-4.
[14] X. Zhang, L. Sun, K. Zhao, and L. Sun, "Nonlinear Speed Control for PMSM System Using Sliding-Mode Control and Disturbance Compensation Techniques," *IEEE Transactions on Industrial Electronics*, vol. 28, no. 3, pp. 1358 - 1365, 2013.
[15] S. S. Rashinkar and S. S. Sankeshwari, "Sliding-mode controller based indirect vector control ofinduction motor," *International Journal of Advances in Engineering & Technology*, 2014.
[16] Z. H. Salih, K. S. Gaeid, and A. Saghafinia, "Sliding Mode Control of Induction Motor with Vector Control in Field Weakening," *Modem Applied Science*, vol. 9, no.2, 2015.

Ngo Thi Hong Huong was born in 1992 in Vietnam, She received her M. E. degree in Electrical Engineering from HCM city University of Technology and Education, Vietnam, in 2019. She is currently working as a lecturer in Faculty of Electrical Technology, Dong An Polytechnic.
Email: ngothihonghuong1992@gmail.com. ORCID: https://orcid.org/0009-0007-9217-4516

Nguyen Minh Tam was born in Vietnam, in 1971. He is the current lecturer at the Control Engineering and Automation Department. He is the current Dean of Faculty of Electrical and Electronic Engineering at Ho Chi Minh City University of Technology and Education, Vietnam. He received the B.E degree in Electrification and Electrical Power Supply from Ho Chi Minh City University of Technical Education, Vietnam, the Masters degree in Electrical Engineering from Ho Chi Minh City University of Technology, Vietnam and the Ph.D. degree in Engineering Science from the University of Technology, Sydney in 1995, 2003 and 2010 respectively. His research interests include system modelling, intelligent and robust control, and soft-computing. Email: tamnm@hcmute.edu.vn.

Nguyen Vinh Quan was born in Vietnam, in 1963. He received his M. E. degree in Automation from HCM city University of Technology, VNU-HCMC, Vietnam, in 2011. He had also received the Ph. D. degree in Power systems from HCM city University of Technology, VNU-HCMC, Vietnam, in 2020. He is currently working as a lecturer in Faculty of Electrical and Electronics Engineering, HCM city University of Technology and Education. His research interests are circuit design, power electronics control, and embedded systems. Email: quannv@hcmute.edu.vn.